

A Study on Recycling of Spent Mushroom Substrate to Prepare Chars and Activated Carbon

Yuhui Ma,^a Qunhui Wang,^{a,*} Xiaohong Sun,^b Xiaoqiang Wang,^c Wei Su,^a and Na Song^a

Chars were obtained from spent mushroom substrate (SMS) via pyrolysis. It was found that as the pyrolysis temperature increased from 400 to 700 °C, the char yield decreased from 45.10 to 33.79 wt.% and the higher heating value increased from 17.32 to 22.72 MJ/kg. The largest BET surface area (13 m²/g) was created at 500 °C. Hydrogen atoms were continuously lost during pyrolysis, whereas oxygen atoms were difficult to eliminate. Whewellite, calcite, lime, and quartz were the minerals in the chars, and their forms and crystallinity changed with changing pyrolysis temperature. Activated carbon with a BET surface area of 1023 m²/g and a total pore volume of 0.595 cm³/g was obtained from the char prepared at 500 °C. Its characteristics were studied by N₂-adsorption, Fourier transform infrared spectroscopy (FTIR), and X-ray diffraction (XRD). The pyrolysis and KOH-activation processes were investigated by thermogravimetric analysis (TGA). The results showed that the pyrolysis of SMS occurred primarily between 217 and 375 °C and that the energies needed for the pyrolysis reactions were relatively low due to the prior mushroom cultivation. Furthermore, lignin was incompletely decomposed in the char prepared at 500 °C, and KOH suppressed tar evolution and reduced the energy needed to decompose the residual lignin during activation.

Keywords: Spent mushroom substrate; Pyrolysis; Char; Activated carbon; Thermogravimetric analysis; Kinetics

Contact information: a: Department of Civil and Environment Engineering, University of Science and Technology Beijing, Beijing 100083, China; b: Beijing Agricultural Biotechnology Centre, Beijing Academy of Agriculture and Forestry, Beijing 100083, China; c: National Engineering Laboratory for Biomass Power Generation Equipment, School of Renewable Energy, North China Electric Power University, Beijing 102206, China; *Corresponding author: txzz709@163.com; wangqh59@sina.com

INTRODUCTION

Biomass Waste Utilization

According to the forecasts from the International Energy Agency (IEA), world primary energy demand is projected to increase from 12150 million tonnes of oil equivalent (Mtoe) in 2009 to 16950 Mtoe in 2035 in the New Policies scenario, an increase of 40%, or 1.3% per year. The global energy demand increases more quickly in the Current Policies scenario, reaching 18300 Mtoe in 2035, 51% higher than 2009, and representing average growth of 1.6% per year (IEA 2011). Among the numerous clean energy generation technologies, the exploitation of biomass is interesting since it is clean and low-carbon. According to the US Environmental Protection Agency (USEPA), biomass contains stored energy because plants absorb energy from the sun through the process of photosynthesis. The bioenergy conversion process, such as burning, releases carbon dioxide. However, plants also take carbon dioxide out of the atmosphere and use it to grow their leaves, flowers, branches, and stems. That same carbon dioxide is

returned to the air when the plants are utilized as fuel (USEPA 2013). Typically, waste biomass is landfilled or incinerated, which incurs a disposal cost and contributes to land or air pollution. The development of bioenergy can minimize the problems associated with the disposal of biomass waste (González *et al.* 2009; USEPA 1996). The Ministry of Science and Technology (MOST) of China has deemed the conversion of industrial biomass waste into useful products one of the top priorities of the 12th Five-Year Plan of Waste Recycling Engineering Science and Technology (MOST 2012).

Lignocellulosic biomass (wood, agricultural residues, forestry residues, energy crops, *etc.*) is the most abundant organic material on earth and has enormous potential as a feedstock for the production of fuel, heat, and electrical power. Biological and thermochemical conversions are two major technologies used for the modification of biomass. Compared to biological processes, thermochemical treatments have the advantages of short processing times and high product yields. Moreover, the thermochemical methods are best suited for dry biomass (moisture content < 10%), which is rich in lignin (this substance is less suited for biochemical conversion since it is hardly broken down by enzymatic activity), such as wood and agricultural wastes (Van de Velden *et al.* 2010). Biomass can be thermochemically transformed *via* direct combustion, gasification, co-gasification with coal, or pyrolysis. Pyrolysis is an attractive way of producing biofuels and is very efficient compared to the other methods (López *et al.* 2013). Generally, the pyrolysis products include biochar, bio-oil, and biogas, and the yields of them change with the pyrolysis process parameters. To predict the yields of the products, some research on the kinetics and reaction modeling has been done and achieved remarkable results (Van de Velden *et al.* 2008, 2010).

Currently, most attention is being paid to the liquid and gaseous products of pyrolysis, which have high caloric values and can be used as fuels. However, due to the complex composition and high acidity of the bio-oil, it cannot be used directly, instead requiring further purification. The low yield and complicated separation and purification processes associated with the gaseous product limit its practical mass-production. Thus, high-value applications of biochar could increase the efficiency of biomass usage (Liu *et al.* 2013). Biochar is a carbonaceous solid and is well known to be an effective soil amendment agent due to its good moisture retention and nutrient holding capacity (González *et al.* 2009), it can reduce the CO₂ and N mineralization, and increase the amount of bacterial biomass in soil (Prayogo *et al.* 2013). Biochar can also be burned, either alone or in combination with other fuels, for energy (López *et al.* 2013). One interesting alternative is the application of char as a precursor for producing activated carbons *via* physicochemical activation (Bernardo *et al.* 2012). Activated carbons are submicroscopically porous materials that are able to adsorb certain amounts of compounds in the liquid and gaseous phases. This makes these solids interesting for use in many industrial applications (Wang *et al.* 2013).

Spent Mushroom Substrate (SMS) in China

Spent mushroom substrate is a by-product of the mushroom production industry. Mushroom substrate, used as growth media to produce mushrooms, is generally composed of straw, hay, corncobs, cotton seed hulls, and some other materials (Hubbe *et al.* 2010). After several mushroom harvesting cycles, the productivity of the mushroom substrate decreases, and the substrate is declared “spent”. Because of biological nitrogen fixation and enzymatic conversion after a certain number of mushroom cultivation cycles, its crude protein content can be increased about 59%, and the fat content may be more

than double, while its cellulose content decreases by about 46%; lignin content, by 63%; and hemicellulose content, by 77% (Gong *et al.* 2012; Guo and Chorover 2006; Li *et al.* 2001; Zhu *et al.* 2012).

China is now the largest producer of mushrooms, accounting for more than 70% of the world's mushroom production (Zhang and Li 2013). The Chinese Academy of Agricultural Sciences reported that the annual production of mushrooms was about 28 million tons in 2012 (Meng 2014). For every kilogram of mushrooms grown, approximately 4 to 5 kg of SMS is produced (Law *et al.* 2003; Medina *et al.* 2012; Phan and Sabaratnam 2012; Uzun 2004). In China, the disposal of SMS is carried out in one of several ways.

The first is careless discarding. Some SMS has always been carelessly discarded by mushroom producers in rural China, causing environmental issues such as mildew reproduction (Liu *et al.* 2008) and water contamination (Liu 2009).

The second is direct burning. Most of the SMS in China is burnt for energy, which is neither environmentally-friendly nor economically optimal (Zhu *et al.* 2013). It is estimated that the combustion of SMS produces ash of more than 10% of its original volume (Finney *et al.* 2009).

Spent mushroom substrate is also used as an animal feed. Since the crude protein and fat contents increase in the mushroom substrate after cultivation, SMS can be used as an animal feed. However, SMS needs to be nutritionally improved before it is fed to animals. It is difficult to store because it is wet and putrefies quickly (Kwak *et al.* 2008). Moreover, the pesticide residues and mildew in SMS are harmful to livestock, leading to safety concerns (Zhang *et al.* 2012).

The final use of SMS is for soil enrichment. Spent mushroom substrate can be used as an organic agricultural fertilizer, but the high content of mineral salts limits its use for the fertilization of salt-sensitive plants. Further, leaching of SMS can seriously endanger local water supplies (Finney *et al.* 2009).

Because SMS is a lignocellulosic material, it can be converted into char and char-based activated carbon *via* pyrolysis and activation. Pyrolysis and activation are thermal-chemical processes based on a series of complex reactions. Thus, it is crucial to understand the mechanism and kinetics by which pyrolysis and activation operate for the practical design of reactors (Slopiecka *et al.* 2012). Previously, there has been no study regarding the preparation of SMS char and char-based activated carbon or the thermal behaviors and kinetics of the pyrolysis and activation processes.

Objectives

The objectives of this study were to produce chars from SMS and evaluate the textural characteristics of the chars produced; to produce activated carbon from SMS-derived char with KOH as the activation agent; to determine the properties of the activated carbon; and to investigate the pyrolysis and kinetic behaviors of SMS and analyze the mechanism and kinetics of the KOH activation process.

EXPERIMENTAL

Materials

The SMS investigated in this study was collected from a mushroom cultivation base located in the Daxing district in the southern part of Beijing, China. Prior to use, the

sample was dried in an oven at 85 °C for 4 h. The dried SMS was crushed and sieved to 80- to 100-mesh particles before further use. The properties of the SMS are given in Table 1.

Table 1. Elemental Composition of SMS

Elemental Composition (wt.%)	C	H	N	O*	S	Atomic H/C	Atomic O/C	Empirical Formula	HHV (MJ/kg)
SMS	39.08	5.29	1.39	53.82	0.42	1.62	1.03	CH _{1.62} N _{0.03} O _{1.03} S _{0.004}	13.86
*Estimated by difference									

Methods

Preparation of chars and activated carbon

The dried, sieved SMS was heated at a temperature increasing by 5 °C/min to final pyrolysis temperatures of 400, 500, 600, or 700 °C in a nitrogen atmosphere (99.995%). The final pyrolysis temperature was maintained for 2 h. The resulting chars were denoted C400, C500, C600, and C700, respectively.

Char C500 was impregnated with KOH solution (42.8 wt.%) using a C500/KOH weight ratio of 1/3 (on a dry basis) and was kept at 30 °C for 30 min. The mixture was then vacuum-filtered, and the solid obtained was dried in an oven. Finally, the solid (denoted KSC) was heated at 800 °C for 90 min in a nitrogen (99.995%) purged tube furnace (OTF-1800X; Kejing, China) with a heating rate of 10 °C/min. The activated product was cooled under nitrogen flow and washed first with 1 M HCl and then with deionized water until the pH of the filtrate became constant. The final product was denoted SAC.

Characterization methods

Elemental analysis was performed with an elemental analyzer (CHNS-932, LECO; USA). The surface area and pore characteristics were analyzed using a gas adsorption apparatus (QuadraSorb SI, Quantachrome Instruments; USA). The BET equation was used to calculate the total surface area and average pore diameter. The total pore volume was estimated from a single N₂ adsorbance point at a relative pressure of about 0.99. Density functional theory (DFT) was used to analyze the successive pore size distribution curve from micropores to macropores. The microspore and mesopore size distributions were deduced using the Horvath-Kawazo (HK) and Barret-Joyner-Halenda (BJH) methods, respectively. The higher heating value (HHV) was measured with an automatic oxygen bomb calorimeter (ZDHW-6H; Yongxin, China). The morphology of the products was analyzed using a scanning electron microscope (SEM) (JSM-6501A, JEOL; Japan). The possible chemical functional groups in the samples were investigated by Fourier transform infrared spectroscopy (FTIR) (Nicolet 6700, Thermo Fisher Scientific; USA). X-ray diffraction (XRD) analysis was carried out using an X-ray diffractometer (D_{max}-RB, Rigaku; Japan). Thermogravimetric analysis was carried out with a thermogravimetric analyzer (HCT-3, Hengjiu; China). Spent mushroom substrate

was heated from room temperature to 800 °C in a nitrogen atmosphere at a heating rate of 5 °C/min. Char C500 and KSC were heated at a rate of 10 °C/min.

Kinetic theory

The rate of reaction for the decomposition of a solid depends on the temperature and the amount of substance present. The rate equation used for the kinetics analysis was (Lu *et al.* 2013),

$$\frac{dx}{dt} = k \cdot f(x) \quad (1)$$

where k is the rate constant, $f(x)$ is a hypothetical model of the reaction mechanism, and x represents conversion ratio of biomass material, defined as,

$$x = \frac{m_0 - m_t}{m_0 - m_\infty} \quad (2)$$

where m_0 is the initial mass of the biomass sample, m_t is the mass at temperature T , and m_∞ is the final mass at the end of pyrolysis. The rate constant can be derived from the Arrhenius equation,

$$k = A \cdot \exp\left(-\frac{E_a}{RT}\right) \quad (3)$$

where A is the pre-exponential factor, E_a is the activation energy, R is the universal gas constant (8.314 J/K·mol), and T is the temperature. The reaction model in Eq. (1) can be expressed as,

$$f(x) = (1-x)^n \quad (4)$$

where n is the order of the reaction. In many applications, the thermal degradation of a solid is assumed to be a first-order reaction ($n = 1$) (Çepelioğullar and Pütün 2013).

Therefore, under a constant heating rate $\beta = dT/dt$, Eq. (1) can be rearranged to,

$$\frac{dx}{dT} = \frac{A}{\beta} \cdot \exp\left(-\frac{E_a}{RT}\right) \cdot (1-x) \quad (5)$$

By application of Coats-Redfern's approximation (Coats and Redfern, 1964), Eq. (5) can be integrated, yielding,

$$\ln\left[-\frac{\ln(1-x)}{T^2}\right] = \ln\left(\frac{AR}{\beta E_a}\right) - \frac{E}{RT} \quad (6)$$

The $\ln[AR/\beta E_a]$ term can be considered a constant. Thus, a straight line can be obtained from a plot of $\ln[-\ln(1-x)/T^2]$ versus $1/T$. From the linear regression of Eq. (6),

the activation energy and the pre-exponential factor can be calculated as the slope and the intercept of the line, respectively.

RESULTS AND DISCUSSION

Characterization of Chars

Char yield as a function of pyrolysis temperature is shown in Fig. 1a. The char yield rapidly decreased, by 8.67%, as the temperature was increased from 400 to 500 °C. However, there was a much more gradual decrease, from 36.33 to 33.79%, as the temperature was increased from 500 to 700 °C.

The BET surface areas of the various chars obtained from the pyrolysis of SMS are presented in Fig. 1b. The surface area reached a maximum of 13 m²/g at 500 °C. The BET surface area created at 400 °C was small because the release of volatiles at this temperature were insignificant in terms of pore development. As the pyrolysis temperature increased to 500 °C, the evolution of volatile products progressively increased, increasing pore formation. The decrease in surface area with further increases in temperature to 600 and 700 °C could be due to sintering at high temperature, followed by shrinkage of the char and realignment of the carbon structure, resulting in reduced surface areas.

To examine the changes in atomic composition, the atomic H/C and O/C ratios of SMS and the chars were plotted in a Van Krevelen diagram, as illustrated in Fig. 1c. The H/C and O/C ratios of SMS were far higher than those of the chars due to the low degree of aromaticity in the biomass structure. Pyrolysis removed hydrogen and oxygen atoms from the SMS and decreased its H/C and O/C values, resulting in the development of the aromatic structure of the chars. The H/C ratio decreased continuously with increasing temperature: the H/C ratios of C500, C600, and C700 were 0.77, 0.55, and 0.32, respectively. In contrast, the O/C ratio did not change significantly across the pyrolysis temperature range of 500 to 700 °C, indicating that the oxygen atoms in C400 were firmly combined with the carbon atoms.

The trends of the changes in the HHVs of the chars can be seen in Fig. 1d. As the pyrolysis temperature increased, the HHV gradually increased, reaching a maximum of 22.72 MJ/kg at 700 °C. The HHV of C700 was higher than that of lignite (15 MJ/kg), and similar to that of subbituminous coal (21 MJ/kg), but lower than that of biodiesel (41 MJ/kg), anthracite (30 MJ/kg), and bituminous coal (27 MJ/kg) (Demirbas 2008; Patzek and Croft 2010).

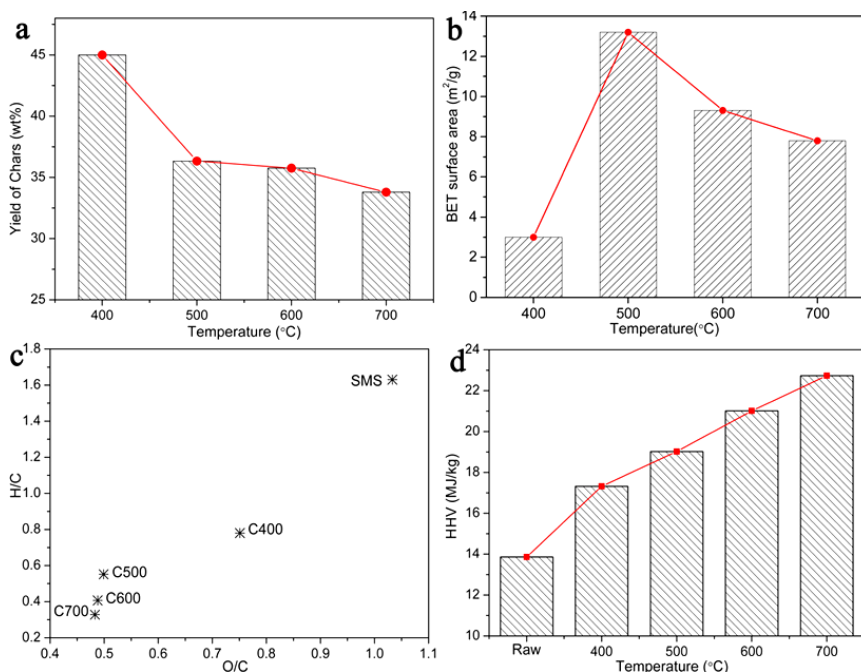


Fig. 1. (a) Product yields for C400, C500, C600, and C700; (b) BET surface areas of C400, C500, C600, and C700; (c) Van Krevelen diagram for SMS and chars obtained at different temperatures; and (d) higher heating values of C400, C500, C600, and C700

Figures 2a through 2d show SEM images of the chars produced at different temperatures. The pyrolysis temperature caused substantial changes to the surface morphology of the chars. C400 had a smooth, planar surface with few pores. C500 had a rough surface with many pores and deep cracks because a dramatic release of different volatile compounds occurred as the temperature increased, leading to the formation of its loose structure. C600 and C700 had relatively dense surfaces due to the collapse of pores and structural shrinkage at high pyrolysis temperatures, which made them more friable or brittle. These results confirm the BET surface area test results.

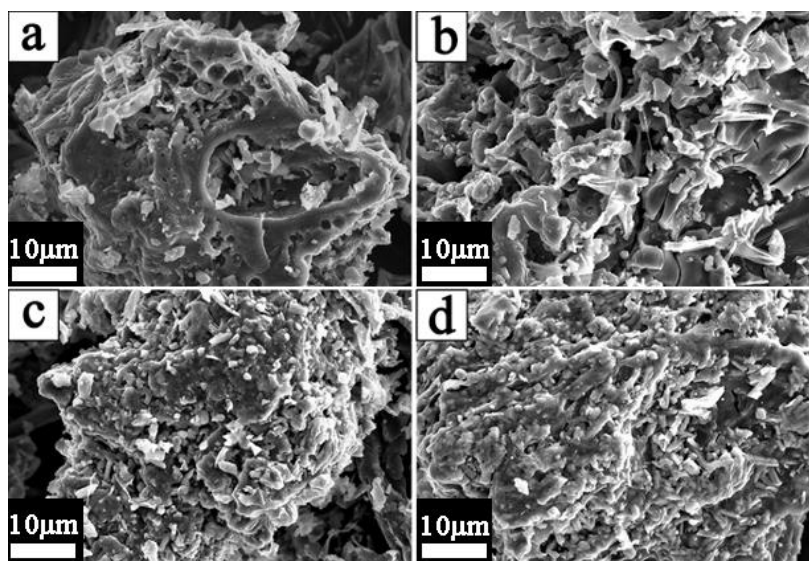


Fig. 2. SEM images of (a) C400, (b) C500, (c) C600, and (d) C700

FTIR spectra recorded for the chars can be seen in Fig. 3a. The functional groups identified from the FTIR spectra are given in Table 2. The absorption peaks at 1635 and 1315 cm^{-1} in the C400 pattern were absent in the patterns of C500, indicating the complete volatilization of oxygen-containing groups due to the increasing pyrolysis temperature. As for C500, an absorption peak at 1590 cm^{-1} was observed, indicating the presence of polynuclear aromatic compounds. However, the intensity of this peak slightly decreased in C600 and C700, possibly due to the realignment of the aromatic structures. The absorption peaks at 1416 and 873 cm^{-1} , representing aromatic C-H vibration, intensified as the pyrolysis temperature was increased from 400 to 500 $^{\circ}\text{C}$, indicating the formation of polynuclear aromatic compounds. However, the two peaks decreased in intensity as the temperature was increased to 600 $^{\circ}\text{C}$ and subsequently to 700 $^{\circ}\text{C}$, possibly due to the loss of hydrogen atoms during pyrolysis at high temperatures. Pyrolysis temperature had no significant effect on the intensity of the absorption peak at 1049 cm^{-1} , which was attributed to C-O stretching. Since SMS has high oxygen content, this phenomenon can be explained by the possibility that the intense interaction between oxygen and carbon during pyrolysis led to their firm combination.

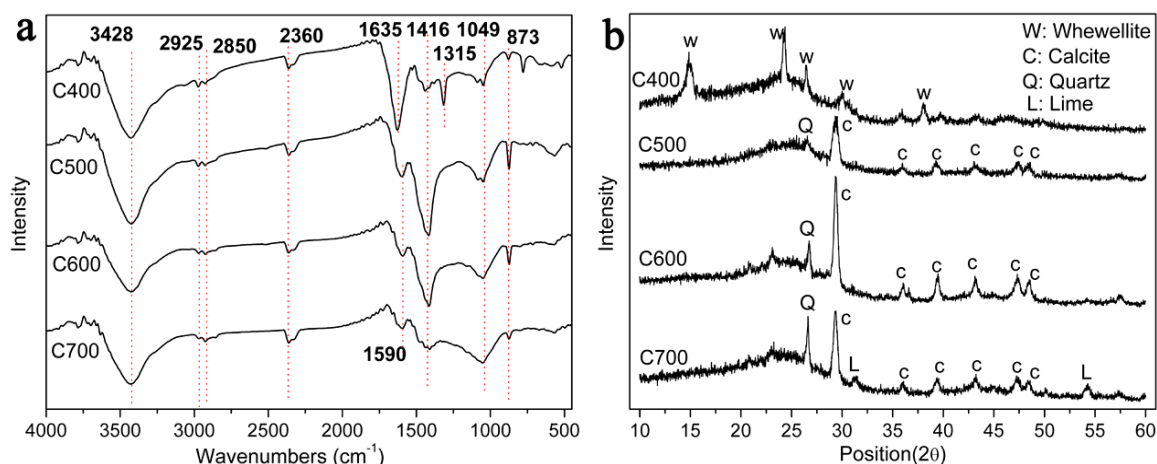


Fig. 3. (a) FTIR spectra for C400, C500, C600, and C700 and (b) XRD patterns of C400, C500, C600, and C700

Table 2. Infrared Band Assignments for the Chars

Wavenumber (cm^{-1})	Description
3420	-OH stretching in phenols and alcohols
2925	Aliphatic CH_3 stretching in alkanes
2850	Aliphatic CH_2 stretching in alkanes
2360	C=O asymmetric stretching vibration of CO_2
1635	C=O stretching (acid, aldehyde and ketone)
1590	In-plane skeletal vibrations in aromatic rings
1416	Aromatic C-H vibration
1315	In-plane bending vibration of phenolic -OH
1049	C-O (anhydrides) stretching
873	Out-plane bending vibration of aromatic C-H

The X-ray diffraction patterns of the chars are shown in Fig. 3b. All of the chars had peaks situated at approximately 24° (2θ), corresponding to the mineralogical phase of graphite. The main inorganic matter in C400 was whewellite ($\text{CaC}_2\text{O}_4 \cdot \text{H}_2\text{O}$), which is usually found in herbaceous plants. However, calcium (Ca) was present as calcite (CaCO_3) in C500, indicating the decomposition of $\text{CaC}_2\text{O}_4 \cdot \text{H}_2\text{O}$ into CaCO_3 and CO at temperatures over 400°C . In addition, with the increase of the pyrolysis temperature from 500 to 600°C , the peaks representing CaCO_3 intensified, indicating that the development of atomic order and crystallite size of CaCO_3 were accelerated by the increasing temperature. However, the CaCO_3 peaks weakened as the pyrolysis temperature increased from 600 to 700°C , possibly due to the decomposition of CaCO_3 into CaO and CO_2 at high temperatures. The emergence of peaks attributed to CaO in C700 confirmed this assumption. Quartz (SiO_2) was also found in C500, C600, and C700. With the increase in pyrolysis temperature from 500 to 700°C , the peak attributed to SiO_2 intensified, indicating that high temperatures favored the development of the crystal structure of SiO_2 .

Characterization of Activated Carbon

The N_2 adsorption/desorption isotherms are shown in Fig. 4a. The SAC shows isotherms similar to Type I-B as defined by IUPAC, indicating the presence of a complex micropore structure. Further, they contained no distinct plateaus even at high relative pressure because some mesopores resulted in a more rapid enhancement near saturation. At higher relative pressures, the hysteresis loop (Type H_4) is indicative of slit-shaped pores. The BET surface area of and total pore volume of SAC were $1023 \text{ m}^2/\text{g}$ and $0.595 \text{ cm}^3/\text{g}$, respectively (see the inset).

The DFT pore size distribution curve of SAC is shown in Fig. 4b. The curve reached a maximum at about 0.9 nm and also had a minor fraction represented by pores of sizes of about 1.0 to 1.6 nm , indicating the presence of supermicropores (diameter between 0.7 and 2 nm). The HK and BJH pore size distribution curves of SAC are presented in the inset. The HK curve had a narrow peak between 0.39 and 0.77 nm , with a maximum at about 0.56 nm , indicating that SAC had the potential for the adsorption of gaseous pollutant molecules (diameter between 0.4 and 0.9 nm). Moreover, the BJH curve reached a maximum at about 3.7 nm , indicating that the mesopores can provide channels for macromolecular adsorbates (*e.g.*, methylene blue) (Yuan *et al.* 2007).

FTIR spectra for SAC are shown in Fig. 4c. Compared to its precursor (C500), SAC had much lower hydrogen content, as shown by the absence of peaks at 1416 and 873 cm^{-1} . However, the strong peak at 1045 cm^{-1} indicated that SAC still had relatively high oxygen content.

The X-ray diffraction pattern of SAC is shown in Fig. 4b. The two broad peaks correspond to the presence of amorphous carbon, associated with the typical turbostratic structure of activated carbon. The absence of a SiO_2 peak after activation can be attributed to KOH impregnation and the reaction between SiO_2 and KOH during the activation process. Moreover, the acid-washing process can remove CaCO_3 from the carbon matrix.

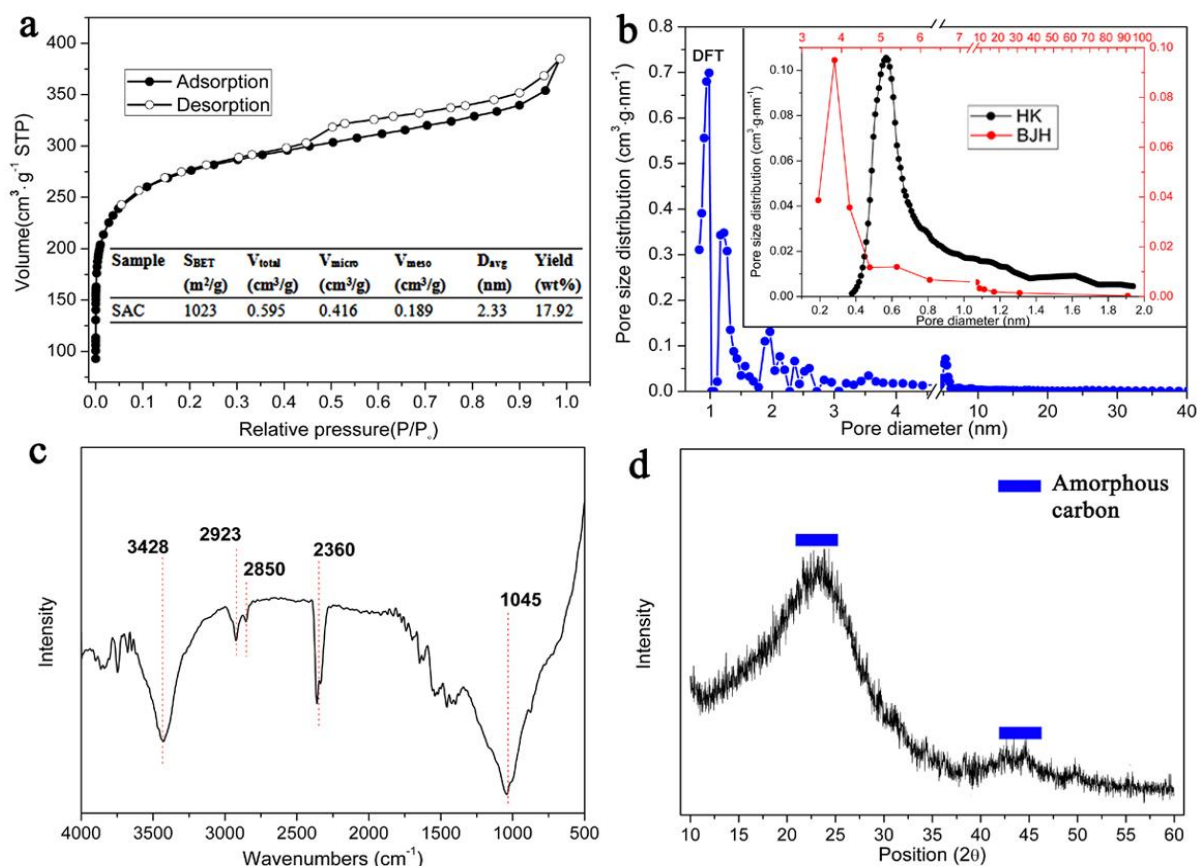


Fig. 4. (a) N_2 adsorption/desorption isotherms of SAC and main textural parameters (inset); (b) DFT pore size distribution of SAC and HK and BJH pore size distribution of SAC (inset); (c) FTIR spectra for SAC; and (d) XRD pattern of SAC

Pyrolysis and Activation Analysis

Pyrolysis of SMS

The TG and Derivative thermogravimetric (DTG) curves of SMS are shown in Fig. 5a. The weight loss below 100°C was attributed to the loss of adsorbed water; the weight loss between 120 and 200°C may have been due to decomposition of small organic molecules in SMS, such as amino acids and fatty acids, generated by the cultivation process; the most significant weight loss, between 200 and 375°C , was mainly due to the pyrolysis of hemicellulose and cellulose in the SMS; the weight loss between about 450 and 510°C indicated the decomposition of $\text{CaC}_2\text{O}_4 \cdot \text{H}_2\text{O}$ into CaCO_3 and CO ; the peak between 600 and 700°C was attributed to the decomposition of CaCO_3 into CaO and CO_2 .

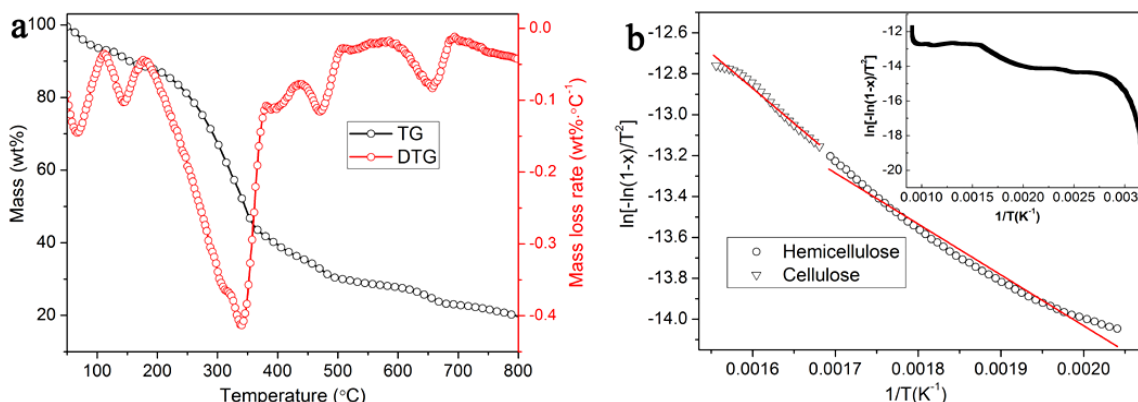


Fig. 5. (a) TG and DTG curves of SMS; (b) plots of $\ln[-\ln(1-x)/T^2]$ versus $1/T$ for the primary pyrolysis of SMS and plots of $\ln[-\ln(1-x)/T^2]$ versus $1/T$ for the pyrolysis of SMS (inset)

The slopes of the $\ln[-\ln(1-x)/T^2]$ versus $1/T$ curves were used to calculate the kinetic parameters. The two sections that constitute the main pyrolysis process of SMS were selected (Fig. 5b). The inset shows the complete $\ln[-\ln(1-x)/T^2]$ versus $1/T$ curve of SMS. The kinetic parameters for the selected sections are listed in Table 3. The energies needed to break down the structure of SMS were lower than those of biomasses in other studies (Çepelioğullar and Pütün 2013; Huang *et al.* 2011). It could be that lignocellulose was degraded to some extent during the mushroom cultivation process.

Table 3. Kinetic Analysis of SMS Pyrolysis

Sample	Temperature (°C)	Conversion (%)	E_a (kJ/mol)	R^2
SMS	217 to 317	17.72 to 48.74	20.69	0.9806
	317 to 375	48.74 to 71.98	28.45	0.9832

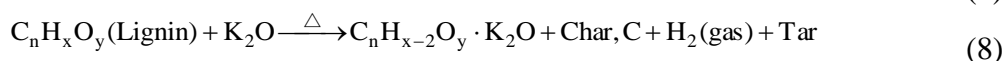
Activation of char

The TG curves of C500 and KSC are shown in Fig. 6a. The C500 curve displayed no significant weight loss below 300 °C because the cellulose and hemicellulose had already fully decomposed during the pyrolysis process. However, an obvious decrease in weight occurred between 305 and 572 °C, which may have been caused by polycondensation of the remaining lignin. The primary weight loss stage of KSC took place between 350 and 550 °C. Thus, KOH impregnation had no significant effect on the temperature range in which the main decomposition process occurred. However, KSC resisted complete decomposition to nearly 750 °C, and there was hardly any weight loss above 572 °C for C500. The KSC residue rate (53.55%) was much higher than that of C500 (32.21%).

As can be seen in Fig. 6b, the degradation of C500 reached a maximum rate of 0.45 %/°C at 419 °C. However, the maximum decomposition rate of KSC, 0.20 %/°C, was achieved at a higher temperature (478 °C). These results indicated that KOH can suppress tar evolution. It is likely that various free radicals were generated during the heating process, and that tar was formed *via* the interaction between the aromatic, macromolecule free radicals and hydrogen free radicals. When KOH was introduced into C500, some of the hydrogen atoms in the lignin were replaced by potassium atoms and became more inclined to escape as H₂ during activation. Thus, there was growing interaction between the aromatic macromolecule free radicals, leading to the

formation of the networks of aromatic rings and a high residue rate. In addition to the main weight loss stage, KSC also had three minor weight loss stages located at 103, 150, and 630 °C, which can be attributed to the loss of moisture, the decomposition of KOH, and the reaction between carbon and water vapor, respectively. The subtle shoulder peak beyond 750 °C could be due to the evaporation of potassium atoms.

Based on the above analysis, a possible activation mechanism is proposed,



The $\ln[-\ln(1-x)/T^2]$ versus $1/T$ curves of C500 and KSC are shown in Fig. 6c. Figure 6d shows the main sections of the two curves. The kinetic parameters of the selected sections can be seen in Table 4. The energy needed to break down the lignin structure of KSC was much lower than that of C500; thus, KOH had a catalytic effect on the decomposition of the residual lignin.

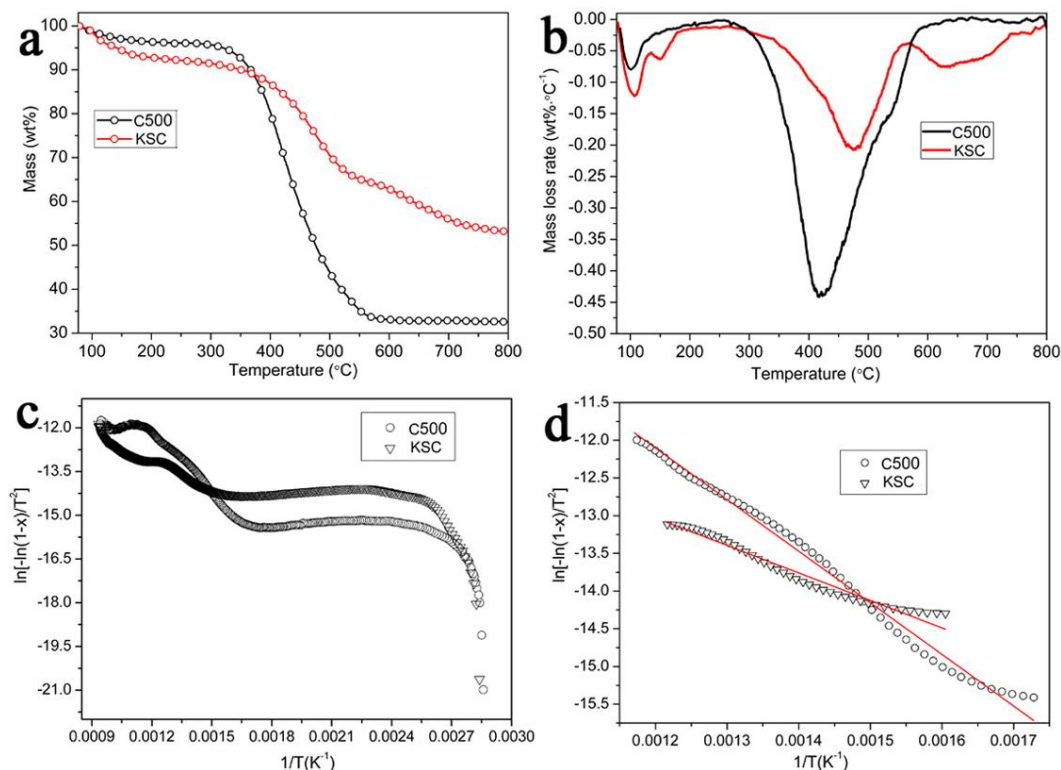


Fig. 6. (a) TG and DTG curves of C500 and KSC; (b) DTG curves of C500 and KSC; (c) plots of $\ln[-\ln(1-x)/T^2]$ versus $1/T$ for the thermal processes of C500 and KSC; and (d) plots of $\ln[-\ln(1-x)/T^2]$ versus $1/T$ for the primary thermal processes of C500 and KSC

Table 4. Kinetic Analysis of Activation Process

Sample	Temperature (°C)	Conversion (%)	E_a (kJ/mol)	R^2
C500	305 to 572	6.41 to 96.82	56.91	0.9917
KSC	350 to 550	21.26 to 74.39	30.33	0.9716

CONCLUSIONS

- Chars were prepared from spent mushroom substrate *via* pyrolysis at different temperatures. As the pyrolysis temperature increased from 400 to 700 °C, the higher heating value of the chars increased from 17.32 to 22.72 MJ/kg. The char prepared at 500 °C had the maximum BET surface area of 13 m²/g. FTIR results showed that hydrogen atoms were lost continuously during pyrolysis. However, oxygen atoms were difficult to remove, indicating the formation of firm bonds between carbon and oxygen during pyrolysis.
- XRD analysis showed that CaC₂O₄·H₂O was the main mineral present in the char prepared at 400 °C; CaCO₃ was the main mineral in the chars prepared at 500 and 600 °C; in the char prepared at 700 °C, CaO was observed due to the decomposition of CaCO₃; SiO₂ was also found in the chars prepared at 500, 600, and 700 °C; and increasing pyrolysis temperature favored the development of the crystal structure of SiO₂.
- Activated carbon was obtained from the char prepared at 500 °C using KOH as the activation agent. The N₂-adsorption analysis showed that the activated carbon had a BET surface area of 1023 m²/g and a total pore volume of 0.595 cm³/g. Further, it primarily consisted of micropores with diameters smaller than 1.6 nm. Some important characteristics of the product were also revealed by FTIR and XRD.
- Thermogravimetric analysis results showed that the primary pyrolysis process of spent mushroom substrate occurred at temperatures between about 217 and 375 °C and that the activation energies of the hemicellulose and cellulose obtained by the Coats-Redfern method were 20.69 and 28.45 kJ/mol, respectively. The energies needed to break down the structure of spent mushroom substrate were relatively low because it was degraded to some extent during the previous cultivation process.
- Lignin was incompletely decomposed in the char prepared at 500 °C. Tar evolution can be suppressed by KOH during activation, leading to a higher residue rate than following the pyrolysis of char alone. It was suggested that the hydrogen atoms in lignin may have been replaced by potassium atoms during the activation process, leading to a high degree of interaction between aromatic macromolecule free radicals and causing char formation. In addition, KOH can reduce the energy needed for the decomposition of the residual lignin in the char.

ACKNOWLEDGMENTS

This work was financially supported by the Environmental Public Welfare Industry Special Scientific Research of China (No. 201209025) and the building of edible fungi innovative team of Beijing (NO. PXM2011-036204-00153). The first author wishes to thank Ms. Jianhua Bian, Ms. Jinghong Mao, and Ms. Hongxia Fan at USTB for their assistance with sample testing.

REFERENCES CITED

- Bernardo, M., Lapa, N., Gonçalves, M., Mendes, B., Pinto, F., Fonseca, I., and Lopes, H. (2012). "Physico-chemical properties of chars obtained in the co-pyrolysis of waste mixtures," *Journal of Hazardous Materials* 219-220, 196-202.
- Çepelioğullar, Ö., and Pütün, A.E. (2013). "Thermal and kinetic behaviors of biomass and plastic wastes in co-pyrolysis," *Energy Conversion and Management* 75, 263-270.
- Coats, A. W., and Redfern, J. P. (1964). "Kinetic parameters from thermogravimetric data," *Nature* 210, 68-69.
- Demirbas, A. (2008). "Relationships derived from physical properties of vegetable oil and biodiesel fuels," *Fuel* 87(8-9), 1743-1748.
- Finney, K. N., Ryu, C., Sharifi, V. N., and Swithenbank, J. (2009). "The reuse of spent mushroom compost and coal tailings for energy recovery: Comparison of thermal treatment technologies," *Bioresource Technology* 100(1), 310-315.
- Gong, F., Zhang, D., Zhang, Y., Han, M., Sun, X., and Li, J. (2012). "The nutritional value and safety assessment analysis on spent mushroom substrate of *pleurotus ostreatus*," *China Animal Husbandry & Veterinary Medicine* 39(11), 86-89 (in Chinese).
- González, J. F., Román, S., Encinar, J. M., and Martínez, G. (2009). "Pyrolysis of various biomass residues and char utilization for the production of activated carbons," *Journal of Analytical and Applied Pyrolysis* 85(1-2), 134-141.
- Guo, M., and Chorover, J. (2006). "Leachate migration from spent mushroom substrate through intact and repacked subsurface soil columns," *Waste Management* 26(2), 133-140.
- Huang, Y. F., Kuan, W. H., Chiueh, P. T., and Lo, S. L. (2011). "Pyrolysis of biomass by thermal analysis-mass spectrometry (TA-MS)," *Bioresource Technology* 102(3), 3527-3534.
- Hubbe, M. A., Nazhad, M., and Sánchez, C. (2010). "Composting as a way to convert cellulosic biomass and organic waste into high value soil amendments: A review," *BioResources* 5(4), 2808-2854.
- IEA. (2011). "World Energy Outlook 2011," <http://www.worldenergyoutlook.org/publications/weo-2011/> [accessed March 31, 2014].
- Kwak, W. S., Jung, S. H., and Kim, Y. I. (2008). "Broiler litter supplementation improves storage and feed-nutritional value of sawdust-based spent mushroom substrate," *Bioresource Technology* 99(8), 2947-2955.
- López, F. A., Centeno, T. A., García-Díaz, I., and Alguacil, F. J. (2013). "Textural and fuel characteristics of the chars produced by the pyrolysis of waste wood, and the

- properties of activated carbons prepared from them," *Journal of Analytical and Applied Pyrolysis* 104, 551-558.
- Law, W. M., Lau, W. N., Lo, K. L., Wai, L. M., and Chiu, S. W. (2003). "Removal of biocide pentachlorophenol in water system by the spent mushroom compost of *Pleurotus pulmonarius*," *Chemosphere* 52(9), 1531-1537.
- Li, Y., Li, X., and Li, H. (2001). "Nutrition analysis and application of waste material of *Lentinus edodes* strain production in *P. Leurotus ostreatu.s* strain production," *Journal of Microbiology* 21(3), 59-60 (in Chinese).
- Liu, H. (2009). "Utilization of spent mushroom substrate in China," <http://www.cefa.org.cn/html/2009/10/14/181.html> [accessed March 4, 2014] (in Chinese).
- Liu, W., Yao, T., Sun, L., and Fan, L. (2008). "The feasibility of spent mushroom substrate as a kind of microbial fertilizer carrier," *Journal of Agro-Environment Science* 231, 94-102 (in Chinese).
- Liu, Z. G., Quek, A., Kent Hoekman, S., and Balasubramanian, R. (2013). "Production of solid biochar fuel from waste biomass by hydrothermal carbonization," *Fuel* 103, 943-949.
- Lu, K.-M., Lee, W.-J., Chen, W.-H., and Lin, T.-C. (2013). "Thermogravimetric analysis and kinetics of co-pyrolysis of raw/torrefied wood and coal blends," *Applied Energy* 105, 57-65.
- Medina, E., Paredes, C., Bustamante, M.A., Moral, R., and Moreno-Caselles, J. (2012). "Relationships between soil physico-chemical, chemical and biological properties in a soil amended with spent mushroom substrate," *Geoderma* 173-174, 152-161.
- Meng, X. (2014). "The first 973 Program in the field of edible mushroom has been started," <http://www.caas.net.cn/ysxw/xzhd/234806.shtml> [accessed March 4, 2014] (in Chinese).
- MOST. (2012). http://www.most.gov.cn/tz/tg/201206/t20120618_95075.htm [March 2, 2014] (in Chinese).
- Patzek, T. W., and Croft, G. D. (2010). "A global coal production forecast with multi-Hubbert cycle analysis," *Energy* 35(8), 3109-3122.
- Phan, C.-W., and Sabaratnam, V. (2012). "Potential uses of spent mushroom substrate and its associated lignocellulosic enzymes," *Applied Microbiology and Biotechnology* 96(4), 863-873.
- Prayogo, C., Jones, J. E., Baeyens, J., and Bending, G. D. (2013). "Impact of biochar on mineralisation of C and N from soil and willow litter and its relationship with microbial community biomass and structure," *Biology and Fertility of Soils*, DOI: 10.1007/s00374-013-0884-5.
- Slopiecka, K., Bartocci, P., and Fantozzi, F. (2012). "Thermogravimetric analysis and kinetic study of poplar wood pyrolysis," *Applied Energy* 97, 491-497.
- USEPA. (1996). <http://www2.epa.gov/green-chemistry/1996-academic-award> [accessed March 31, 2014].
- USEPA. (2013). "Biomass Energy," <http://www.epa.gov/climatechange/kids/solutions/technologies/biomass.html> [accessed March 31, 2014].
- Uzun, I. (2004). "Use of spent mushroom compost in sustainable fruit production," *Journal of Fruit and Ornamental Plant Research* 12, 157-165.

- Van de Velden, M., Baeyens, J., and Boukis, I. (2008). "Modeling CFB biomass pyrolysis reactors," *Biomass and Bioenergy* 32(2), 128-139.
- Van de Velden, M., Baeyens, J., Brems, A., Janssens, B., and Dewil, R. (2010). "Fundamentals, kinetics and endothermicity of the biomass pyrolysis reaction," *Renewable Energy* 35(1), 232-242.
- Wang, X., Li, D., Li, W., Peng, J., Xia, H., Zhang, L., Guo, S., and Guo, C. (2013). "Optimization of mesoporous activated carbons from coconut shells by chemical activation with phosphoric acid," *BioResources* 8(4), 6184-6195.
- Yuan, X., Liu, Y., Zhuo, S., Xing, W., Sun, Y., Dai, X., Liu, X., and Yan, Z. (2007). "Synthesis of ordered mesoporous carbon and its application in aqueous macromolecular adsorption," *Acta Chimica Sinica* 65(17), 1814-1820 (in Chinese).
- Zhang, C., Yan, J., Zhang, J., and Kuang, S. (2012). "Study on the nutritive value of oyster mushroom bran," *China Feed* (3), 13-15 (in Chinese).
- Zhang, X., and Li, H. (2013). "China has become the largest producer of mushroom in the world," http://news.xinhuanet.com/local/2013-05/21/c_115845229.htm [accessed March 4, 2014] (in Chinese).
- Zhu, H.-J., Liu, J.-H., Sun, L.-F., Hu, Z.-F., and Qiao, J.-J. (2013). "Combined alkali and acid pretreatment of spent mushroom substrate for reducing sugar and biofertilizer production," *Bioresource Technology* 136, 257-266.
- Zhu, H., Sheng, K., Yan, E., Qiao, J., and Lv, F. (2012). "Extraction, purification and antibacterial activities of a polysaccharide from spent mushroom substrate," *International Journal of Biological Macromolecules* 50(3), 840-843.

Article submitted: March 13, 2014; Peer review completed: March 28, 2014; Revised version accepted: April 3, 2014; Published: May 13, 2014.